doi:10.1093/brain/awaa076 BRAIN 2020: 143; 1350–1367 | 1350

BRAIN
A JOURNAL OF NEUROLOGY

In vivo stress granule misprocessing evidenced in a *FUS* knock-in ALS mouse model

Xue Zhang,[1,2,3,4] Fengchao Wang,[5] Yi Hu,[2,4] Runze Chen,[1,2,3,4] Dawei Meng,[1,2,3,4] Liang Guo,[1,2,3,4] Hailong Lv,[1,2,3,4] Jisong Guan[6] and Yichang Jia[1,3,4]

Many RNA-binding proteins, including TDP-43, FUS, and TIA1, are stress granule components, dysfunction of which causes amyotrophic lateral sclerosis (ALS). However, whether a mutant RNA-binding protein disrupts stress granule processing *in vivo* in pathogenesis is unknown. Here we establish a *FUS* ALS mutation, p.R521C, knock-in mouse model that carries impaired motor ability and late-onset motor neuron loss. In disease-susceptible neurons, stress induces mislocalization of mutant FUS into stress granules and upregulation of ubiquitin, two hallmarks of disease pathology. Additionally, stress aggravates motor performance decline in the mutant mouse. By using two-photon imaging in TIA1-EGFP transduced animals, we document more intensely TIA1-EGFP-positive granules formed hours but cleared weeks after stress challenge in neurons in the mutant cortex. Moreover, neurons with severe granule misprocessing die days after stress challenge. Therefore, we argue that stress granule misprocessing is pathogenic in ALS, and the model we provide here is sound for further disease mechanistic study.

1 Tsinghua-Peking Joint Center for Life Science, Beijing, China
2 School of Life Sciences, Tsinghua University, Beijing, China
3 School of Medicine, Medical Science Building, Room D204, Tsinghua University, Beijing, China
4 IDG/McGovern Institute for Brain Research at Tsinghua Beijing, China
5 Animal core facility, National Institute of Biological Sciences, Beijing, China
6 School of Life Science and Technology, Shanghai Tech University, Shanghai, China

Correspondence to: Yichang Jia, PhD
School of Medicine, Medical Science Building, Room D204, Tsinghua University, Beijing
100084, P. R. China
E-mail: yichangjia@tsinghua.edu.cn

Keywords: ALS; FUS-R521C; stress granule; knock-in; mouse model

Abbreviations: ALS = amyotrophic lateral sclerosis; AS = sodium arsenite; ChAT = choline acetyltransferase; FTD = frontotemporal dementia; RBP = RNA-binding protein; RMI = relative mean intensity

Introduction

Mutations in genes encoding two structurally similar RNA-binding proteins (RBPs), TDP-43 (encoded by *TARDBP*) and FUS, are associated with amyotrophic lateral sclerosis (ALS) and frontotemporal dementia (FTD), two neurodegenerative disorders sharing genetic and pathological overlap (Ling *et al.*, 2013; Renton *et al.*, 2014). More strikingly, ubiquitin-positive and mislocalized TDP-43 and FUS are found in a large proportion of ALS and FTD cases, underscoring RBP dysfunction in the pathogenesis (Lagier-Tourenne *et al.*, 2010; Ling *et al.*, 2013; Renton *et al.*, 2014).

Recently, TDP-43 and FUS, among many other RBPs that contain low complexity domain, have been identified in a

Received April 19, 2019. Revised January 10, 2020. Accepted February 2, 2020. Advance access publication May 1, 2020

cytoplasmic mRNA/protein complex, also known as stress granules, which often appear under stress conditions to temporarily cease cytoplasmic mRNA translation initiation (Kedersha *et al.*, 2005; Buchan *et al.*, 2013; Kim *et al.*, 2013; Li *et al.*, 2013; Aulas and Vande Velde, 2015; Molliex *et al.*, 2015). Like *TARDBP* and *FUS*, mutations in the RBP genes have also been linked to neurodegenerative diseases, including ALS and FTD (Elden *et al.*, 2010; Kim *et al.*, 2013; Aulas and Vande Velde, 2015; Mackenzie *et al.*, 2017). In ALS and FTD patient tissues, TDP-43 co-localized with stress granule markers, and in cultured cells, overexpressed mutant TDP-43 and FUS were found in stress granules induced by various stresses (Colombrita *et al.*, 2009; Bosco *et al.*, 2010; Liu-Yesucevitz *et al.*, 2010). Mutations in *VCP*, a gene encoding a protein involved in autophagic clearance of stress granules, have been closely associated with ALS and FTD (Buchan *et al.*, 2013). Indeed, ubiquitin-positive inclusion-containing mislocalized RBP is a pathological hallmark of ALS/FTD (Dormann and Haass, 2011; Renton *et al.*, 2014; Harrison and Shorter, 2017). Taken together, these data argue that the misprocessing of stress granules may contribute to disease aetiology.

In the past, efforts have been made to generate animal models of ALS by overexpressing recombinant DNA carrying mutations found in ALS families. Although those transgenic animal models provided significant insights into the disease mechanisms, there may also be potential artefacts driven by ectopic overexpression of mutant proteins in the disease models (Gurney *et al.*, 1994; Jonsson *et al.*, 2006; Swarup and Julien, 2011). Indeed, overexpression of wild-type TDP-43 and FUS generate similar motor phenotypes to those of the mutant transgenes in many animal species, including fly, mouse, and rat (Lagier-Tourenne *et al.*, 2010; Huang *et al.*, 2011; Swarup *et al.*, 2011; Mitchell *et al.*, 2013; Qiu *et al.*, 2014). The transgenic strategy has other caveats, including uncertain genome insertion sites, unstable copy numbers, potential disruption of genome integrity, ectopic expression pattern driven by exogenous promoter, and lack of endogenous splicing regulation.

Disease mutation knock-in approaches avoid the major caveats seen in the transgenic disease models and closely reflect the disease nature. Initial efforts have been made to generate knock-in mouse models for ALS and these animal models provide significant insights into the disease development and mechanisms underlying mutation-associated neurodegeneration. By introducing ALS and its relevant mutations into mouse endogenous *Tardbp*, studies have revealed late-onset motor neurodegeneration, early stage ALS pathologies, and RNA metabolism abnormalities in the knock-in mutant animals (Fratta *et al.*, 2018; White *et al.*, 2018; Ebstein *et al.*, 2019). Using a similar approach, late-onset motor neuron loss, mitochondria abnormality, and both cell autonomous and non-cell autonomous mutant FUS toxicities have been documented in mutant FUS knock-in ALS models (Devoy *et al.*, 2017; Scekic-Zahirovic *et al.*, 2017). Although stress granule misprocessing has been proposed to be involved in the aetiology, little is known regarding whether dysfunction of RBPs through stress granule misprocessing leads to motor neurodegeneration *in vivo* and whether a stress challenge is able to accelerate disease manifestation and induce disease pathology in these rational ALS models.

In the current study, we selected a frequent and highly penetrant ALS-associated FUS mutation, FUS-R521C to generate a knock-in mouse model for ALS. Three reasons prompted us to choose FUS-R521C to generate a knock-in ALS mouse model. First, the R521C mutation is located in the FUS C-terminus, a non-classical PY nuclear localization signal (NLS), in which more than half of ALS-associated *FUS* mutations are clustered (Dormann *et al.*, 2010; Dormann and Haass, 2011). Second, the R521C mutation has been found in both familial and sporadic ALS patients in a geographically unrelated manner with high disease penetrance (Kwiatkowski *et al.*, 2009; Vance *et al.*, 2009; Suzuki *et al.*, 2010; Yamamoto-Watanabe *et al.*, 2010; Drepper *et al.*, 2011; Swarup *et al.*, 2011; Sproviero *et al.*, 2012). Third, FUS-R521C transgenic mice and rats present some disease-relevant phenotypes (Huang *et al.*, 2011; Qiu *et al.*, 2014; Lopez-Erauskin *et al.*, 2018). Aged knock-in mice show motor axon degeneration, and motor neuron loss, and a decline in motor ability. The knock-in mutant mouse and its isogenic wild-type control allow us to ask whether, under stress conditions, the endogenous level of mutant RBP leads to disease through disruption of normal stress granule processing. In motor neuron culture, after stress challenge, the mutant, but not wild-type FUS preferentially moves into stress granules and results in more stress granule formation and less stress granule disassembly. In the mutant knock-in mouse, stress induces a severe decline in motor ability, FUS mislocalization into cytoplasmic stress granules, and ubiquitin upregulation. The latter two are pathological hallmarks seen in ALS patients. To trace the stress granule processing *in vivo*, we tagged TIA1 (a stress granule marker) with EGFP and monitored EGFP granule processing before and after stress treatment by two-photon imaging. In the mutant motor cortex, we observed TIA1-positive granule misprocessing and that neurons with severe granule processing defects disappeared after stress challenge. Taken together, we argue that dysfunction of RBPs disrupts stress granule processing in the disease pathogenesis, and the FUS knock-in ALS model we describe here could be a useful mammalian model to study the disease mechanisms underlying neurodegenerative diseases caused by dysfunction of RBPs.

Materials and methods

Knock-in mouse generation and mouse care

To generate the FUS-R521C knock-in mouse, we used the CRISPR-Cas9-based knock-in approach (Platt *et al.*, 2014; Shalem *et al.*, 2015). Because of the shorter length of the mouse

FUS protein, the mouse position corresponding to human R521 is R513. The donor DNA fragment contains the R513C mutation (tcg to ctg) and the flanking left and right homology arms (~1 kb). We used the C57BL/6J (JAX, Stock No. 000664) mouse genomic DNA as template to amplify the arms of donor DNA. The donor DNA, gRNA (gcgagcacagacaggatcgcAGG, PAM site capitalized), and *Cas9* mRNA were injected into C57BL/6J embryos. The injected embryos were transferred into the oviduct ampulla of the pseudo-pregnant ICR (JAX, Stock No. 009122) female recipients. The desired genotype offspring were backcrossed to C57BL/6J for several generations to establish the lines.

The animal facility at Tsinghua University has been fully accredited by the Association for the Assessment and Accreditation of Laboratory Animal Care International (AAALAC) since 2014. All animal protocols were approved by the Institutional Animal Care and Use Committee (IACUC) at Tsinghua University or National Facility for Protein Science in Shanghai based on the Guide for the Care and Use of Laboratory Animals (Eighth Edition, NHR). The C57BL/6J and ICR mice were purchased from Charles River Laboratories, Beijing, China. All mice were housed in isolated ventilated cages (maximum six mice per cage) barrier facility at Tsinghua University or National Facility for Protein Science in Shanghai. The mice were maintained on a 12/12-h light/dark cycle, 22–26°C, 40–70% humidity with sterile pellet food and water *ad libitum*. Cages were checked daily to ensure animal welfare. Body weight was assessed regularly to ensure no weight loss. Where animals were used for research, we followed the 3Rs (replacement, refinement or reduction) rules.

Mouse behaviour tests

For the open field behaviour test, the single animal was placed in the centre of an open field area (60 × 60 cm) and tracked with multiple parameters, including total distance, average speed, and distance travelled in the centre region using the TopScan behavioural analysis system (CleverSys) at a 10-min interval (Chew *et al.*, 2015). Anxiety levels were measured by distance travelled in the centre region divided by total distance travelled (Chew *et al.*, 2015). Vertical rearing activity was measured by total standing time on hind legs in the 10-min interval of the open field test (Ito *et al.*, 2016). Rotarod performance was measured by an automated system (Med Associates Inc.) (Chew *et al.*, 2015). In brief, the animal was placed on an accelerating spindle (4–40 rpm) for 5 min per trial and three consecutive trials per day for 4 days. A 20-min break was set in between each trial. The fall time from the spindle was auto-calculated by the system when the mouse fell off the spindle within the 5-min interval. The stay time was calculated by subtraction of the fall time from the 5 min, and the mean value of the stay time from three consecutive trials per day was used for statistical analysis. According to the age and genotype, the mice were allocated to different experimental groups. The behaviour assays were performed randomly in wild-type and mutant groups.

Generation and validation of FUS antibody

For generation of FUS antibody, the N-terminal 214 amino acids of mouse *Fus* were cloned and fused with MBP (maltose-binding protein). *Escherichia coli*-expressed FUS-MBP fusion protein was purified by Amylose Resin High Flow (NEB) and condensed by Amicon Ultra-15 Centrifugal Filter Units (Millipore). The subcutaneous inoculation was performed once every 2 weeks for three times (0.1 mg antigen in complete/incomplete Freund's adjuvant per rabbit; Sigma). The resulting rabbit anti-serum was used for antibody characterization.

For the FUS antibody validation, Neuro-2a cells (ATCC CCL-131) were grown in Dulbecco's modified Eagle medium (Corning) plus 10% foetal bovine serum (Hyclone) at 37°C with 5% CO_2. For *FUS* knockdown, the cells were infected with the *FUS* lentivirus-shRNAs (MissionRNAi, Sigma). After 3 days of infection, the infected cells were selected with 1 μg/ml puromycin for 72 h. The puromycin-selected cells were applied for the FUS antibody validation.

Quantitative PCR

Total RNA was extracted from mouse spinal cord with TRIzol® reagent (Invitrogen) and treated with RQ1 RNase-free DNase (Promega) as per the manufacturer's instructions. The treated RNA was reverse-transcribed using M-MLV Reverse Transcriptase (Promega) with oligo(dT) priming. Quantitative PCR was performed using qPCR SYBR® Green Master Mix (Yeasen Biotechnology). Each reaction was performed in triplicate and the mean Cq value was used for calculation. *Gapdh* was used as internal control for mRNA expression normalization.

Femoral nerve dissection, axon count, and ChAT-positive neuron count

Dissection of femoral nerves was performed as described previously (Jia *et al.*, 2015). The femoral nerve was exposed in the sacrificed mice and briefly fixed (2% glutaraldehyde/2% paraformaldehyde in 0.1 M cacodylate buffer) before dissection. The isolated nerves were post-fixed overnight in the same fixative. Dissected nerves were processed for plastic embedding and transmission electron microscopy by standard procedures. Nerve cross sections were stained with toluidine blue and examined by light microscopy. For motor neuron count, lumbar 4 to 5 of spinal cord was dissected and sectioned into 5-μm sections. We did serial sectioning and collected one every 10 sections, and 15–20 collected sections from each spinal cord were used for choline acetyltransferase (ChAT) staining. ChAT-positive neurons of the ventral horn were counted and the average number of motor neurons was calculated.

Haematoxylin and eosin stain

Mice were intracardically perfused with phosphate-buffered saline (PBS) and fixed with Bouin's solution (Sigma) at different time points after arsenite (AS) treatment. Mouse tissues were dissected and post-fixed overnight before paraffin embedding. Tissues were sectioned into 5-μm sections for haematoxylin and eosin staining.

Motor neuron culture and stress challenge

For motor neuron culture, as previously described, the spinal cords were dissected from embryonic Day (E)13.5 mouse embryos and digested with papain (Sigma, 1:200) with EDTA (1 mM) in Neurobasal™ (Invitrogen) at 37°C for 30 min. During the digestion, DNAse I (Sigma, 10 μg/ml) was added in the last 10 min. After digestion, the tissue suspension was passed through a 40-μm strainer. The resulting cell pellet was resuspended in 1 ml HBSS (Invitrogen) with EDTA (0.5 mM), and the suspension was layered over a cushion of 5 ml OptiPrep™ (Sigma, 10%). After centrifugation at 400*g* for 25 min, the motor neurons were enriched in the top 1 ml volume. The motor neurons were grown in Neurobasal™ with B27 (Invitrogen), horse serum (10% v/v; Sigma), GlutaMAX™-1 (Invitrogen), and characterized by immunostaining with anti-ChAT (rabbit, Millipore) and anti-Tuj-1 (mouse, Beyotime) antibodies. For stress granule induction, the cultured motor neurons (3 days *in vitro*) were treated with sodium arsenite (AS, 1 mM) for a time dependent on the experiment purpose.

Arsenite intragastric administration

The AS solution was administrated by a rounded tip feeding tube at the dose indicated in the experimental procedure and the wild-type and mutant mice were treated randomly. After each administration, the mice were returned to their cages and monitored for at least 5 min. If necessary, animals went through the open field test once every week to monitor their locomotion.

Immunoblot

Tissues or cultured cells were lysed in RIPA buffer (50 mM Tris-HCl, pH 8.0, 150 mM NaCl, 0.25% sodium deoxycholate, 0.1% SDS, 1% NP-40, supplemented with complete protease inhibitor mixture; Roche). Lysates were separated on SDS-PAGE gels and transferred to PVDF membranes (GE Healthcare) using standard techniques. Blots were incubated with the primary antibodies overnight at 4°C, and then HRP-conjugated secondary antibodies at room temperature for 1 h.

Immunostaining and data quantification

For tissue immunostaining, anaesthetized mice were transcardially perfused with PBS and then 4% PFA, and brains were post-fixed in the same fixative before paraffin embedding. Antigen retrieval was performed in 0.01 M citrate buffer, pH 6.0. The brain sections were incubated at 4°C overnight with the primary antibodies: rabbit anti-FUS, mouse anti-ubiquitin (Cell Signaling Technology), mouse anti-NeuN (Millipore), goat anti-eIF3η (Santa Cruz), and goat anti-ChAT (Millipore), mouse anti-G3BP1 (Abcam), rabbit anti-GFAP (Cell Signaling), and rabbit anti-Iba1(Wako). Fluorescent detection was performed with Alexa Fluor-conjugated secondary antibodies (Invitrogen), and images were collected by confocal microscopy.

For cell immunostaining, the cultured cells were fixed with 4% PFA at room temperature for 10 min. After being washed with PBS, the cells were applied for the primary antibodies: rabbit anti-FUS (homemade), goat anti-TIA1 (Santa Cruz), goat anti-eIF3η (Santa Cruz), mouse anti-G3BP (Abcam), rabbit anti-ChAT (Millipore) and mouse anti-Tuj-1 (Beyotime). Following the PBS wash, Alexa Fluor-conjugated secondary antibodies (Invitrogen) were applied.

Images were captured by Nikon A1 confocal microscope. The objective lens was 40×/NA 1.25 or 100×/NA 1.40. Alexa 488 was excited with a 488 nm laser and detected at 500–550 nm. Alexa 555 was excited with a 561 nm laser and detected at 570–620 nm. Alexa 647 was excited with a 638 nm laser and detected at 663–738 nm. Every channel was examined using sequential scanning. The maximum intensity projection images were used for stress granule number, intensity and mean intensity analysis using Fiji (ImageJ). Intensity maps of mutant FUS inside stress granules were generated by MATLAB.

To avoid the variance of whole cell mean intensity across different conditions or among different individual cells, we used relative mean intensity (RMI) to compare the given stress granule component or protein level in different conditions or groups, and used mean intensity to calculate correlation between individual stress granule components. For *in vitro* culture, the RMI = mean intensity of TIA1 and FUS inside stress granules divided by that in nucleus. For spinal cord sections, the RMI = mean intensity of ubiquitin, eIF3η, and G3BP1 divided by mean intensity of background. We used the Pearson's coefficient in each region of interest to measure the co-relationship of fluorescent intensities between two proteins using Imaris.

For GFAP-positive and Iba1-positive cell count, after GFAP and Iba1 immunostaining, the number and intensity of GFAP-positive and Iba1-positive cells were counted using Imaris.

Two-photon *in vivo* imaging and data analysis

Two-photon *in vivo* imaging was carried out as previously described (Xie *et al.*, 2014). The lentiviral particles expressing TIA1-EGFP were injected into the wild-type and mutant M2 motor cortex before the surgery and imaging experimental procedure. Two weeks after the lentiviral infection, the wild-type and mutant mice received cranial window implantation surgery. For the window implantation, the animal was anaesthetized with 1.5% isoflurane and then immobilized using custom-built stage-mounted ear bars. A 1.5-cm incision was made, and the scalp was removed to expose the skull. One circular craniotomy (4-mm diameter) above the bilateral motor cortex was made using a high-speed drill under a dissecting microscope. A glass coverslip was attached to the exposed brain tissue and sealed with dental cement. The space between the coverslip and the tissue was filled with artificial CSF. To avoid the inflammation caused by surgery, we changed the padding every day. To avoid implanted cranial window fall, we housed the mice in a separate single cage. One month after the implantation surgery, the EGFP positive neurons in the motor cortex were imaged with an Olympus Fluoview FVMPE-RS, coupled with a 25× water immersion lens (NA 1.05). Mode-locked titanium/sapphire laser (MaiTai HP DeepSee-OL, Spectra-Physics) generated two-photon excitation at 960 nm and collected emitted light in the range of 500–540 nm. The *z*-stack 2D maximum intensity projection and optical sectioning were generated and analysed using Fiji (ImageJ). RMI = the mean intensity of TIA1-EGFP inside of the granule divided by the whole cell mean intensity of TIA1-EGFP. Imaris was used for 3D reconstruction of TIA1-EGFP granule

and data analysis. The 3D RMI = the sum of mean intensity of TIA1-EGFP inside of the 3D granule volume divided by the sum of mean intensity of TIA1-EGFP in the 3D whole cell. The percentage of TIA1-EGFP granule total intensity = the total TIA1-EGFP granule intensity in the given neuron divided by the overall neuron TIA1-EGFP intensity × 100%.

Data availability

The authors confirm that the data supporting the findings of this study are available within the article and its Supplementary material.

Results

Generation of a knock-in mouse line carrying an ALS FUS-R521C mutation

The C-terminal NLS encoded by the last exon of mouse *FUS* is conserved across species and identical to that of human (515GEHRQDRRERPY526) (Fig. 1A). The mouse position corresponding to human R521 is R513. Downstream of the mouse R513 triplet codon is a PAM site for Cas9 recognition (Fig. 1B). After genome editing, the correct sequence (R513 to C) and germ line transmission of the mutation were confirmed (Fig. 1C and D). Using a mouse FUS antibody (Supplementary Fig. 1), we documented that the mutant FUS expression level was higher than that of wild-type across different tissues, especially with significant upregulation (~3–4-fold) in spinal cord at early and late disease stages (Fig. 1E and Supplementary Fig. 2A). The upregulation of mutant FUS seems not be caused by the expression level of mutant *FUS* mRNA (Supplementary Fig. 2B and C). Therefore, we concluded that we had established a knock-in mouse line carrying an ALS *FUS* mutation.

Impaired motor ability in the knock-in mouse

Unlike early-onset motor disability and death seen in previously reported wild-type and mutant FUS transgenic mice (Wegorzewska *et al.*, 2009; Mitchell *et al.*, 2013; Qiu *et al.*, 2014), we did not observe a progressive paralysis in the knock-in mice up to 2 years of age. We also did not find obvious mislocalization of mutant FUS in ChAT-positive motor neurons in the aged knock-in mice (Supplementary Fig. 3). However, a decline of spontaneous locomotor activity was observed in the 7-month-old heterozygous and homozygous knock-in animals, but not in the younger (4 months of age) knock-in animals (Fig. 2A). The decline in motor ability was further documented by the rearing time, a sensitive measurement for hindlimb muscle strength (Ito *et al.*, 2016). Compared to the wild-type, both heterozygous and homozygous knock-in groups showed significant reduction ($P < 0.01$, ANOVA) in the rearing time at both 4 and 7 months of age (Fig. 2B). Rotarod performance also supported the

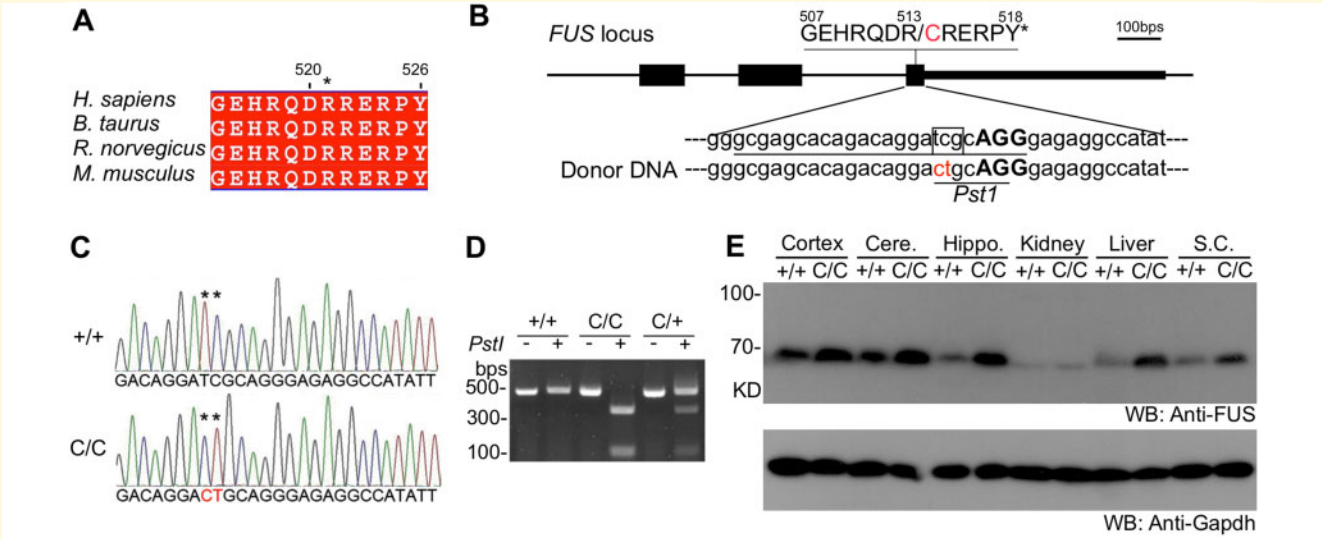

Figure 1 Generation of the FUS-R521C knock-in mouse. (**A**) Alignment of last 12 amino acids of FUS in different mammal species. The amino acids are highly conserved from rodent to human. The human FUS sequences were used as a reference for amino acid positioning. The R521 residue is labelled with asterisk. (**B**) The genome structure of mouse *FUS*. The mouse FUS R513 corresponds to human R521. Two nucleotide mutations labelled in red were introduced into mouse *FUS* locus 2 bp upstream of the PAM site (in bold upper case). The underlined sequences corresponded to gRNA sequences. A novel PstI cutting site was built into the locus for genotyping. (**C** and **D**) DNA chromatograms and PstI digestion confirmed the correct genome insertion. (**E**) The expression of FUS in mouse various tissues. The tissues from wild-type (+/+) and homozygous FUS-R521C knock-in (C/C) mice at 1 month of age were blotted with FUS antibody. Gapdh was used as loading control. Cere. = cerebellum; Hippo. = hippocampus; S.C. = spinal cord.

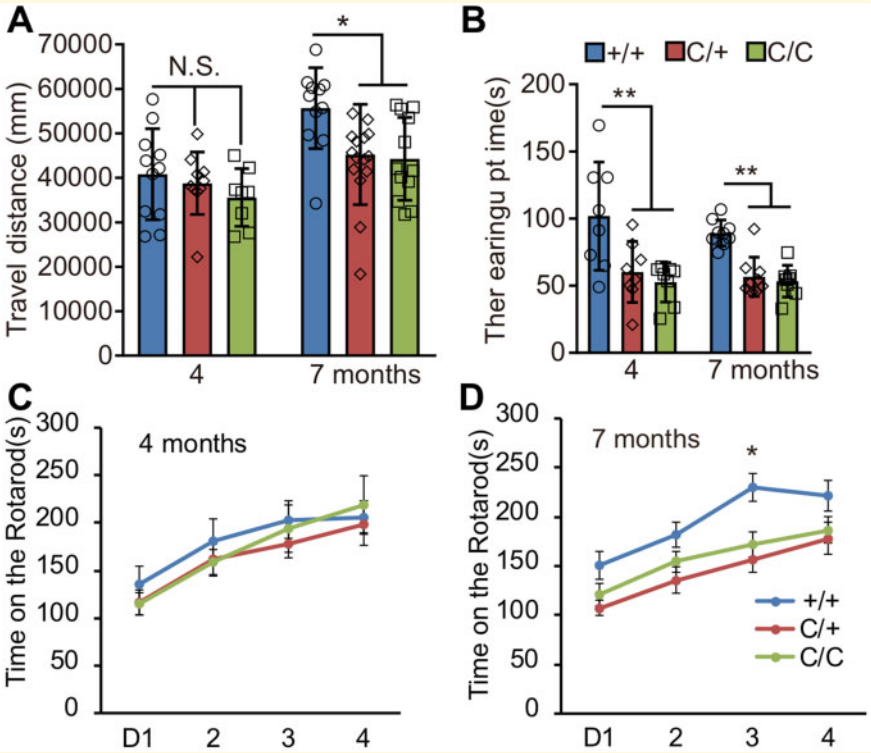

Figure 2 Impairment of motor ability in FUS-R521C mice. (**A**) Open field test in 4- and 7-month-old wild-type (+/+), heterozygous (C/+), and homozygous (C/C) mice. Four months, $n = 8$–11, male; 7 months, $n = 11$–16, male. (**B**) Vertical rearing activity was calculated in 4- and 7-month-old mice. The rearing time was significantly reduced in the heterozygous and homozygous groups, compared to the wild-type group. Four months, $n = 8$, male; 7 months, $n = 8$–9, male. (**C** and **D**) Rotarod test was carried out in wild-type, heterozygous, and homozygous mice at 4 (**C**) and 7 (**D**) months of age. The stay time on the rotarod was significantly decreased in 7-month knock-in (heterozygous and homozygous) mice at Day 3, but not in the younger (4 months) mutant mice. Four months, $n = 7$–8, male. Seven months, $n = 9$–13, male. In **A** and **B**, the values are presented as mean ± standard deviation (SD). In **C** and **D**, the values are presented as mean ± SEM. $^{*}P < 0.05$, $^{**}P < 0.01$ (ANOVA, SPSS). N.S. = no statistical significance.

impaired motor ability in aged (7-month-old) mutant mice, but not in the younger (4-month-old) mutant animals (Fig. 2C and D).

Progressive motor neuron degeneration in the knock-in mouse

In addition to the decline in motor ability in the knock-in mice, there was a corresponding loss of peripheral motor axons. At 8 months of age, degenerating motor axons in the femoral nerve were observed in the heterozygous and homozygous knock-in mutant animals (Fig. 3A). By counting the axon number, we found that the number of large diameter ($\geqslant 5$ μm) fibres, but not small fibres (< 5 μm), were significantly reduced ($P < 0.01$, ANOVA) in the heterozygous and homozygous knock-in mutant mice (Fig. 3B), suggesting that the peripheral fibres with fast conduction velocity are most affected by the expression of mutant FUS. The axon degeneration does not result from motor neuron loss in the mutant mice at 8 months of age, as the number of ChAT-positive motor neurons in the spinal cords was not decreased (Fig. 3C). However, significant motor neuron loss was documented in both heterozygous and homozygous mutant mice at 2 years of age (Fig. 3C and D). In agreement with the observed progressive motor neuron loss, a progressive neuroinflammation, as evidenced by GFAP and Iba1 activation, was documented in the mutant spinal cords (Supplementary Fig. 4). Therefore, we concluded that our ALS *FUS* mutation knock-in mouse displays progressive motor neuron degeneration.

Mutant FUS locates into stress granules and leads to less dynamic stress granules after stress challenge

The formation/disassembly of stress granules is highly context-dependent (Li *et al.*, 2013; Protter and Parker, 2016), and how endogenous levels of ALS mutant FUS affects stress granule processing in ALS-susceptible neurons is largely unknown. To this end, we cultured primary motor neurons from wild-type, knock-in heterozygous, and knock-in homozygous mutant spinal cords (Supplementary Fig. 5). After treatment with AS, an oxidative stress inducer (Liu *et al.*,

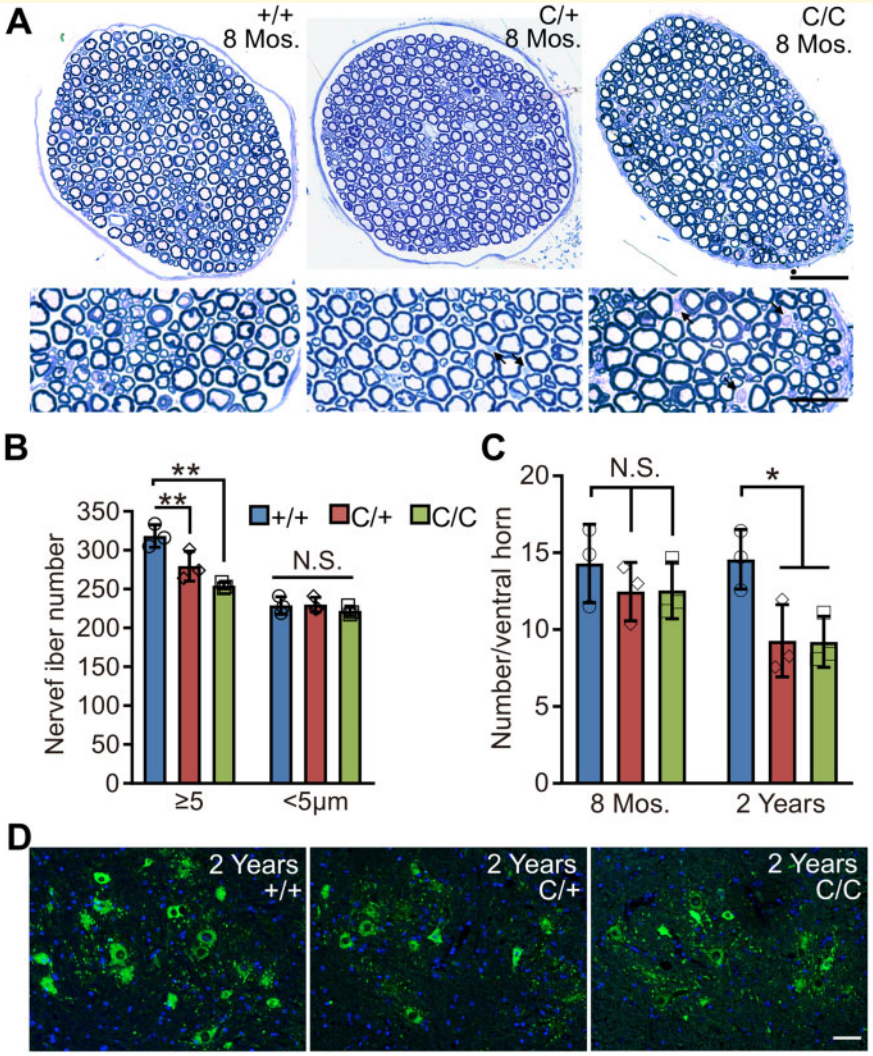

Figure 3 Motor axon degeneration and motor neuron loss shown in the FUS-R521C mice. (**A**) Toluidine blue-stained cross sections of femoral nerve motor branches from wild-type (+/+), heterozygous (C/+), and homozygous (C/C) mice at 8 months of age. Axon degeneration (arrow), but no typical signs of demyelination, was observed as shown in higher magnification images. The diameter of the black dot in low magnification image is 5 μm. (**B**) The big size (diameter ⩾ 5 μm), but not the small size (< 5 μm), nerve fibre number of femoral motor branches was significantly reduced in heterozygous and homozygous mice at 8 months of age ($n \geqslant 3$). (**C**) The number of ChAT-positive motor neurons in the ventral horn of the indicated genotypes at 8 months (Mos.) and 2 years of age. (**D**) The ChAT-positive motor neurons in sections from lumbar 4–5 spinal cords of wild-type, heterozygous, and homozygous mice at 2 years of age. In **B** and **C**, values are presented as mean ± SD. $^{**}P < 0.01$, $^{***}P < 0.001$ (ANOVA, SPSS). N.S. = no statistical significance. In **C**, data comprise three individual animals/condition, and 29–41 slides/condition. Scale bar = 50 μm in **A** in low and 25 μm in high magnification images; 50 μm in **D.**

2001; Shi *et al.*, 2004), the formation of TIA1-positive stress granules was observed in both wild-type and knock-in mutant cultures (Fig. 4A). The mutant stress granules were also positive for G3BP1, another stress granule marker (Supplementary Fig. 6). The percentage of motor neurons containing stress granules and the number of stress granules per cell were increased in the heterozygous and homozygous mutant neurons after AS challenge, indicating that the mutant motor neuron is prone to form stress granules (Fig. 4B and C). Interestingly, nearly all the stress granules were double-positive for TIA1 and FUS in the heterozygous and homozygous mutant cultures. However, double-positive stress granules were rarely seen in wild-type motor neurons, nor was FUS mislocalized into the cytoplasm (Fig. 4A and D). Without AS treatment, no TIA1-positive stress granule or FUS mislocalization was seen in the wild-type and knock-in mutant cultures (Supplementary Fig. 7). Therefore, we concluded that the mutant, but not wild-type FUS, translocates into stress granules and increases stress granule formation after AS challenge.

To study stress granule dynamics, we withdrew the stress treatment and examined stress granule disassembly. In wild-type primary neuron cultures, the number of stress granules per cell was significantly reduced ($P < 0.01$, ANOVA) after

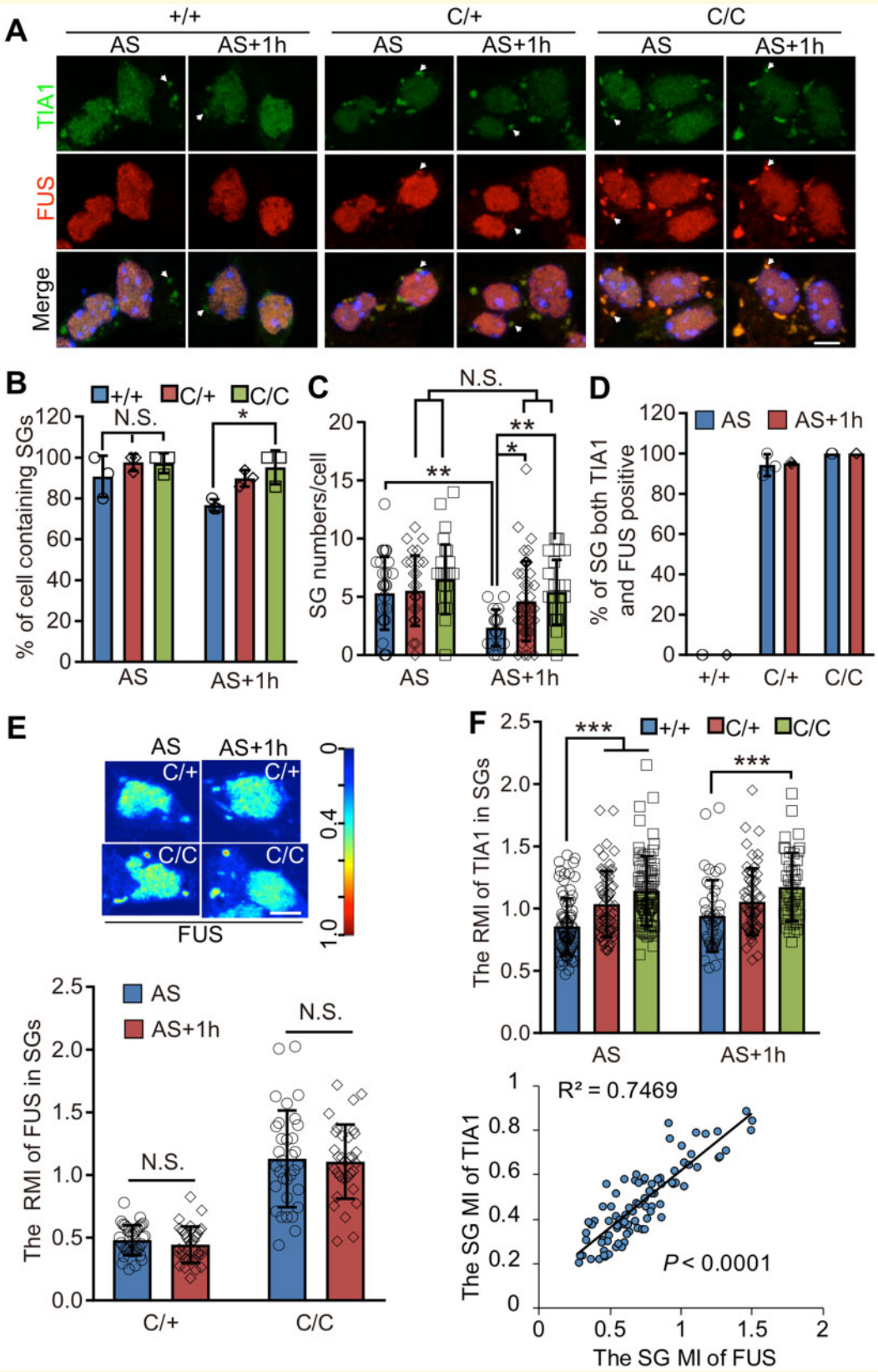

Figure 4 ALS mutant FUS moves into stress granules in cultured motor neuron and leads to mutant stress granule less dynamics after stress challenge. (**A**) Representative immunostaining images from wild-type (+/+), heterozygous (C/+), and homozygous (C/C) cultured motor neurons (3 days *in vitro*) treated with AS (1 mM, 1 h) or recovered from AS treatment (AS + 1h). The typical TIA1-positive stress granules are indicated with arrowheads. The TIA1-positive stress granules were formed in wild-type, heterozygous, and homozygous motor neurons after AS treatment. Note the mutant FUS moves into TIA1-positive stress granules after AS treatment. (**B** and **C**) The statistical

(continued)

1 h of recovery (Fig. 4A and C). However, in the heterozygous and homozygous mutant cultures, the stress granule number showed no significant decrease after recovery (Fig. 4C), indicating that the stress granules containing mutant FUS are defective in disassembly.

Mean intensity was used to estimate the protein level and dynamics inside of the given subcellular compartment (Wheeler *et al.*, 2016; Maharana *et al.*, 2018). However, the variance of whole-cell mean intensity across different conditions or among different individual cells affects the comparison. To reduce variability, we used RMI to compare the given stress granule component level in different conditions or groups, and used mean intensity to calculate correlation between individual stress granule components. The RMI of mutant FUS remained unchanged between the stress treatment and recovery (Fig. 4E), suggesting low dynamics of mutant FUS in stress granules during the stress challenge. The FUS RMI in the heterozygous motor neurons was about half of that in the homozygous condition, supporting the notion that stress induces relocation of ALS mutant FUS into stress granules, but not wild-type FUS. We hypothesized that the relocation of mutant FUS decreases the dynamics of the stress granule, which in turn may lead to more stress granule components retained in the stress granule, including TIA1. Indeed, the TIA1 RMI was higher in the mutant cultures after AS treatment and stress recovery (Fig. 4F). In addition, the stress granule mean intensity of TIA1 was correlated with that of FUS (R^2 = 0.7469). Taken together, by using isogenic cultured motor neurons, we demonstrated that the mutant FUS moves into stress granules when the motor neuron faces a stress challenge, which in turn leads to retention of stress granule components and reduction of stress granule dynamics.

Chronic stress worsens motor impairment and induces disease pathology in the knock-in mutant mouse

As cultured mutant motor neurons have defects in stress granule processing, we next asked whether the chronic stress challenge was able to accelerate disease manifestation in mutant mice. To this end, we exposed knock-in mice to chronic stress by intragastric administration of AS four times a week for 8 weeks (Fig. 5A). After 1- or 2-months exposure to AS, the rearing time was significantly decreased ($P < 0.01$, ANOVA) in the mutant, but not the wild-type group, indicating that a pronounced motor decline is induced by chronic stress in the mutant mice (Fig. 5B). Compared to the wild-type mice, the mutant knock-in mice did not show a decrease in travel distance after the stress exposure (Supplementary Fig. 8A), probably due to strong anxiety-like behaviour induced by the AS treatment in the mutant group (Supplementary Fig. 8B).

The hallmark pathology of ALS is formation of ubiquitin-positive inclusions containing TDP-43 or FUS in cytoplasm in the diseased neurons (Dormann and Haass, 2011; Renton *et al.*, 2014; Harrison and Shorter, 2017). Without stress challenge, we failed to document mislocalized cytoplasmic FUS in the mutant spinal cord or in cultured mutant motor neurons (Supplementary Figs 3 and 7), reminiscent of normal nuclear localization of mutant FUS reported in BAC transgenic mouse lines carrying human *FUS* mutations (Lopez-Erauskin *et al.*, 2018). However, the chronic stress exposure induced FUS cytoplasmic mislocalization in the mutant motor neurons but not in the wild-type neurons, although the wild-type and mutant mice were exposed to the same dose of AS (Fig. 5C). We also documented the upregulation of ubiquitin in the mutant motor neurons (Fig. 5D) and co-localization of cytoplasmic FUS and ubiquitin by Pearson's coefficient (Supplementary Fig. 9A). Therefore, we concluded that the ALS mutant FUS together with chronic stress are both required for aggravation of the motor impairment and induction of the disease pathology.

Cytoplasmic FUS co-localized with stress granule markers in mutant spinal cord after a stress challenge

To examine whether the mislocalized mutant FUS relocated into stress granules in spinal cord, we stained wild-type and knock-in mutant spinal cord sections with an antibody for eIF3η, a stress granule marker and a key subunit of the eukaryotic translation initiation factor 3 (eIF3) complex (Liu-Yesucevitz *et al.*, 2010; Buchan *et al.*, 2013; Becker *et al.*, 2017; Zhang *et al.*, 2018). In motor neuron cultures, both

Figure 4 Continued

results from **A**. The percentage of motor neurons containing stress granules (**B**) and the stress granule number per cell (**C**). (**D**) The percentage of both TIA1- and FUS-positive stress granules after AS treatment (AS) or the recovery (AS + 1h). (**E**) The RMI of mutant FUS in stress granules after AS treatment and recovery. The mean intensity (MI) was calculated by ImageJ. RMI, the mutant FUS mean intensity in the individual granule divided by the FUS nuclear mean intensity of the given neuron. The stress granule RMI of FUS did not change between AS treatment and recovery in both heterozygous, and homozygous groups. Note the RMI of FUS in the heterozygous group was a half of that in homozygous group. The heat map colour represents the mutant FUS intensity. Stress granule characterization and data analysis were done by ImageJ (n = 33–36). (**F**) Compared to the wild-type group, the RMI of TIA1 in the stress granules was higher in the mutant groups (n = 46–83). The stress granule mean intensity of TIA1 was correlated with that of FUS in the homozygous mutant neurons (C/C) treated with AS. The correlation analysis was done by GraphPad Prism 7.04 (n = 88). Scale bar = 5 μm in **A** and **E**. In **B**–**F**, the values are presented as mean ± SD. *$P < 0.05$, **$P < 0.01$, ***$P < 0.001$ (ANOVA or t-test, SPSS). N.S. = no statistical significance. In **C**, at least three independent experiments, n = 17–39.

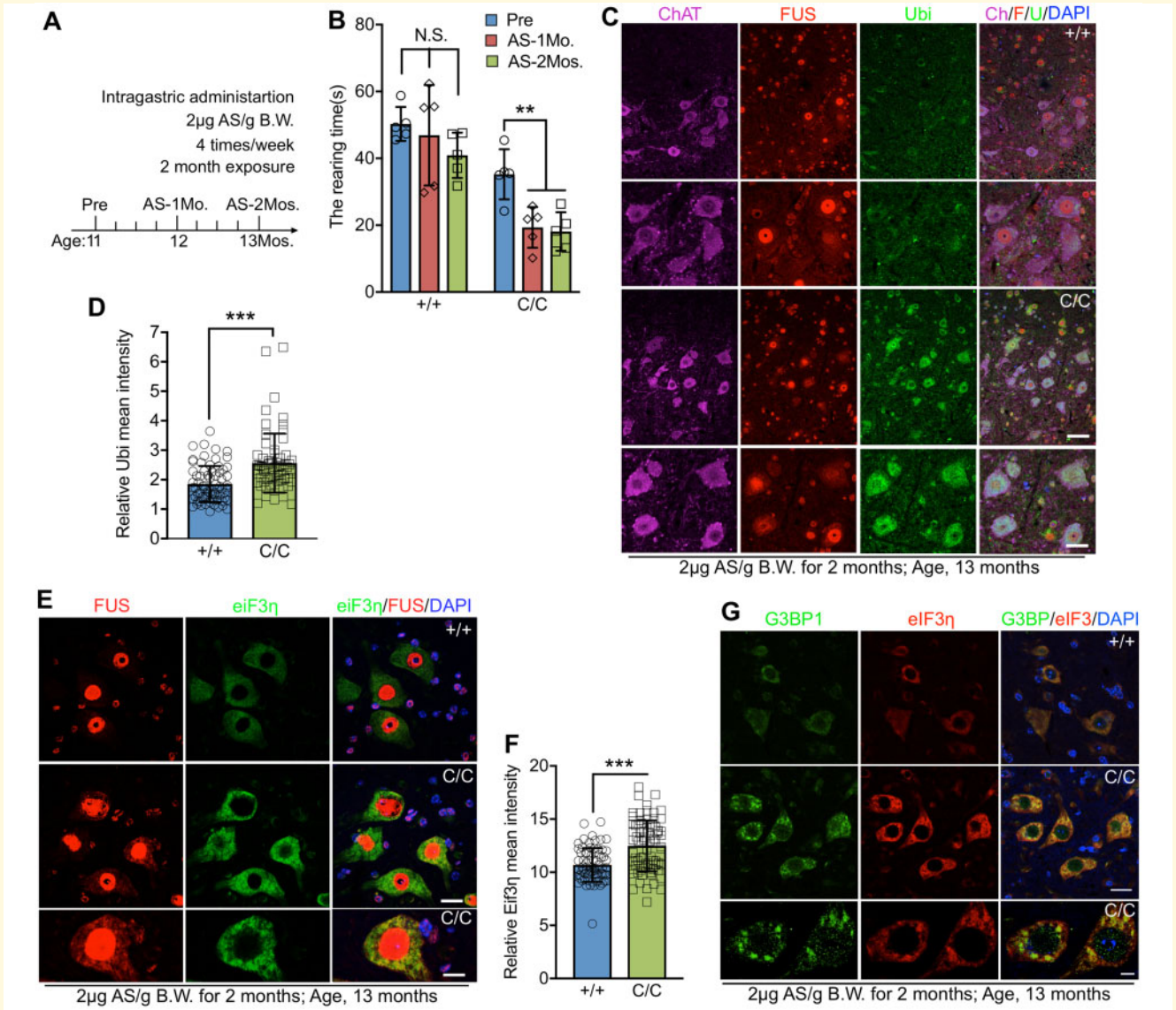

Figure 5 The chronic stress worsens motor impairment and induces the disease pathologies in the knock-in mouse. (**A**) The schedule for intragastric administration of AS in mice. (**B**) The rearing time before and after AS exposure. The significant decrease in rearing time at 1 or 2 months after AS treatment in the knock-in mice. (**C** and **D**) The chronic stress induced mutant FUS mislocalization and ubiquitin upregulation in the ChAT-positive motor neurons in the mutant spinal cord. The RMI of fluorescent signals of ubiquitin (Ubi) (**D**) were measured using ImageJ. (**E** and **F**) The stress treatment induced the upregulation of eIF3η in knock-in mutant spinal cord ventral horn. The co-localization between cytoplasmic mutant FUS and eIF3η was documented in the knock-in mutant spinal cord. The RMI of fluorescent signals of eIF3η (**F**) were measured using ImageJ. (**G**) The stress treatment induced the upregulation of G3BP1 in knock-in mutant spinal cord ventral horn. The co-localization between G3BP1 and eIF3η was documented in the knock-in mutant spinal cord. Sections from lumbar 4–5 spinal cords in **C**, **E** and **G**. Scale bar = 50 μm in **C** in low and 25 μm in high magnification images; 20 μm in low and 10 μm in high magnification images in **E** and **G**, respectively; In **B**, $n = 5$ [wild-type (+/+) and homozygous (C/C), respectively], male. In **D** and **F**, three individual animals/group, 1–2 images/animal. In **D**, $n = 70$ (wild-type) and $n = 65$ (homozygous); in **F**, $n = 71$ (wild-type) and $n = 77$ (homozygous). The values are presented as mean ± SD. $^{**}P < 0.01$, $^{***}P < 0.001$ (*t*-test, ANOVA, SPSS).

eIF3η and mutant FUS appeared in stress granules after stress challenge (Supplementary Fig. 10A). In addition, the mean intensity of eIF3η inside stress granules was correlated with that of mutant FUS ($R^2 = 0.7369$) (Supplementary Fig. 10B), similar to the correlation between TIA1 and mutant FUS (Fig. 4F), supporting the notion that relocation of mutant FUS into stress granules results in other stress granule components being retained in stress granules. Although no obvious eIF3η upregulation was observed in the spinal cords of the aged naïve knock-in mice (Supplementary Fig. 11), the upregulation of eIF3η was induced by the chronic stress treatment in the mutant but not wild-type ventral horns, and the signals were largely co-localized with the mislocalized mutant FUS (Fig. 5E, F and Supplementary Fig. 9B). Similar to

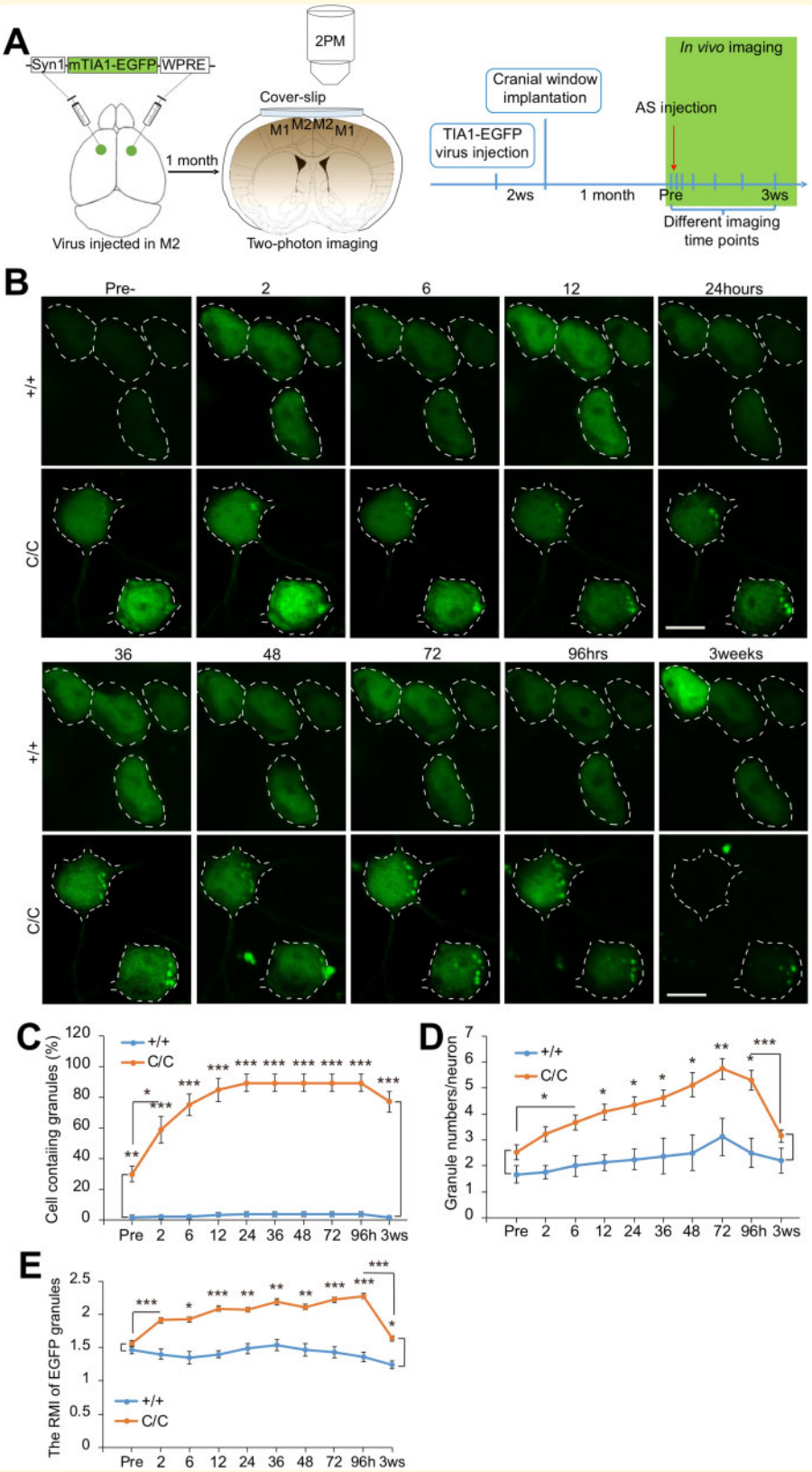

Figure 6 ***In vivo*** **evidence for misprocessing of TIA1-positive granule in the mutant motor cortex.** (**A**) Our experimental setting for monitoring TIA1-positive granule processing *in vivo*. A lentiviral expression system was used for expression of TIA1-EGFP driven by a neuronal promoter Syn1 (*left*). The timeline for the viruses injected into the motor cortex and the EGFP signals monitored at various time points by two-photon imaging (*right*). (**B**) The time-lapse imaging of TIA1-EGFP signals after one dose of AS treatment (4 μg/g body weight) in the 10-month-old wild-type (+/+) and homozygous (C/C) mice. The TIA1-EGFP granules were formed in the homozygous neurons but not in that

(continued)

eIF3η, upregulation of another stress granule marker G3BP1 was induced by the stress treatment in the mutant spinal cords (Fig. 5G and Supplementary Fig. 9C). In addition, more mutant motor neurons (61/75) contain G3BP1-positive granules than the wild-type neurons (4/76) and more G3BP1-positive granules appeared in the mutant neurons after the stress treatment (Supplementary Fig. 9D). Taken together, our data demonstrate that stress granule markers, including eIF3η and G3BP1, are upregulated in the mutant ventral horn after chronic stress challenge, and are co-localized with mislocalized mutant FUS, suggesting that the mutant FUS alters normal stress granule processing in the diseased neuron *in vivo*.

In vivo evidence for TIA1-positive granule misprocessing in the mutant brain

To address whether the expression of mutant FUS affects stress granule processing *in vivo*, we tagged TIA1, a stress granule marker (Kedersha *et al.*, 1999), with EGFP and used two-photon imaging to visualize the EGFP signals *in vivo* (Fig. 6A). We found that when the cultured neurons were infected with the lentiviral particles expressing TIA1-EGF, the EGFP signals of TIA1-EGFP faithfully reflected TIA1 subcellular localization, (Supplementary Fig. 12). In addition, like TIA1, the TIA1-EGFP, but not EGFP, relocated into stress granules after AS stress challenge (Supplementary Fig. 12). We then injected the lentiviral particles into M2 motor cortex and confirmed the neuronal expression of TIA1-EGFP when driven by a neuronal promoter Syn1 (Supplementary Fig. 13).

To induce stress *in vivo*, we applied AS (4 mg/kg body weight) to the mice by intragastric administration. To ensure that the acute toxic effect of AS (4 mg/kg body weight) was limited, we examined animal viability and body weight 4 days after the oral application. A slightly higher dose (6 mg/kg body weight) of AS had little effect on animal viability or body weight in both wild-type and FUS homozygous mutant animals (Supplementary Fig. 14A). Using a similar delivery approach, previous studies have shown that arsenic concentration quickly reaches plateau (within 2–3 h) and drops to baseline 10 h after administration in non-neuronal tissues such as kidney and liver (Flora, 1999; Juarez-Reyes *et al.*, 2009; Li *et al.*, 2017). In contrast, brain concentration reaches plateau ∼8–10 h after AS treatment, and returns to baseline ∼20 h after treatment (Flora, 1999; Juarez-Reyes *et al.*, 2009; Li *et al.*, 2017). In agreement that the acute effect of AS we applied *in vivo* is mild, we did not see obvious morphological changes in kidney, liver, and brain at 2, 8, and 24 h after the treatment (Supplementary Fig. 14B).

After one dose of AS treatment, the TIA1-EGFP granules were documented at various time points in the homozygous mutant motor cortex by optical sectioning and *z*-stack 2D projection (Fig. 6B and Supplementary Video 1). However, granules were barely seen in the wild-type motor cortex. The percentage of neurons containing TIA1-EGFP granules in the mutant motor cortex was significantly increased ($P < 0.001$, *t*-test) after AS challenge (Fig. 6C). The percentage reached a plateau 24 h after one dose of AS challenge in the mutant groups (89.29 ± 5.49%), and the high percentage lasted 96 h after the challenge (Fig. 6C). Three weeks after AS treatment the percentage reduced (77.20 ± 6.72%). These data indicate that the ALS mutant FUS significantly enhances granule formation *in vivo*, and the formation of TIA1-EGFP granules is rapid (hours) and stress-dependent but the disassembly/clearance is much slower (weeks) *in vivo*.

To estimate the TIA1-EGFP granule numbers per neuron and the intensity inside of granules, we used *z*-stack maximum intensity projections (Fig. 6B). Compared to the estimated numbers in the wild-type at various time points, the granule numbers in the mutant group climbed until 72 h, and were then slightly decreased at 96 h (Fig. 6D). However, the number was significantly decreased ($P < 0.001$, *t*-test) 3 weeks after the treatment, indicating that the TIA1-EGFP granules in the mutant motor cortex are indeed disassembled or cleared, but in a slow process compared to that of formation. In contrast, the granule numbers in the wild-type showed no significant change across various time points after AS treatment, supporting the notion that much less TIA1-EGFP granule is formed in the wild-type cortex after stress challenge, at least at current two-photon imaging resolution level.

To compare TIA1-EGFP level inside of the granule across the different time points and different genotypes *in vivo*, we calculated the RMI, as we used in the *in vitro* studies (Fig. 4E and F). The RMI was not different between the wild-type and mutant groups before AS treatment (Fig. 6E). However, 2 h after the challenge, the TIA1 RMI was significantly increased ($P < 0.001$, *t*-test) in the mutant neurons. The RMI was maintained at a high level until 96 h after the treatment in the mutant group. Three weeks later, the RMI reduced to the levels at pretreatment (Fig. 6E). Taken together, our data indicate that the expression of ALS mutant FUS drives more TIA1 moving into the granules shortly after the stress challenge and increases TIA1-positive granule

Figure 6 Continued

of wild-type after the treatment. Note a TIA1-EGFP positive neuron disappeared 3 weeks after treatment in homozygous mutant motor cortex. Scale bar = 10 μm. (**C**–**E**) The percentage of neurons containing the TIA1-EGFP granules (**C**), the average of granule numbers in the given neuron containing granule(s) (**D**), and the average of TIA1-EGFP RMI (**E**). RMI is given by the TIA-EGFP mean intensity of individual granule divided by the TIA1-EGFP mean intensity of the given neuron. The values are presented as mean ± standard error of the mean (SEM). For wild-type, three male animals, seven areas, and 177 EGFP-positive neurons; for homozygous mutant, three male animals, 10 areas, and 104 EGFP-positive neurons. $^{*}P < 0.05$, $^{**}P < 0.01$, $^{***}P < 0.001$ (*t*-test, SPSS).

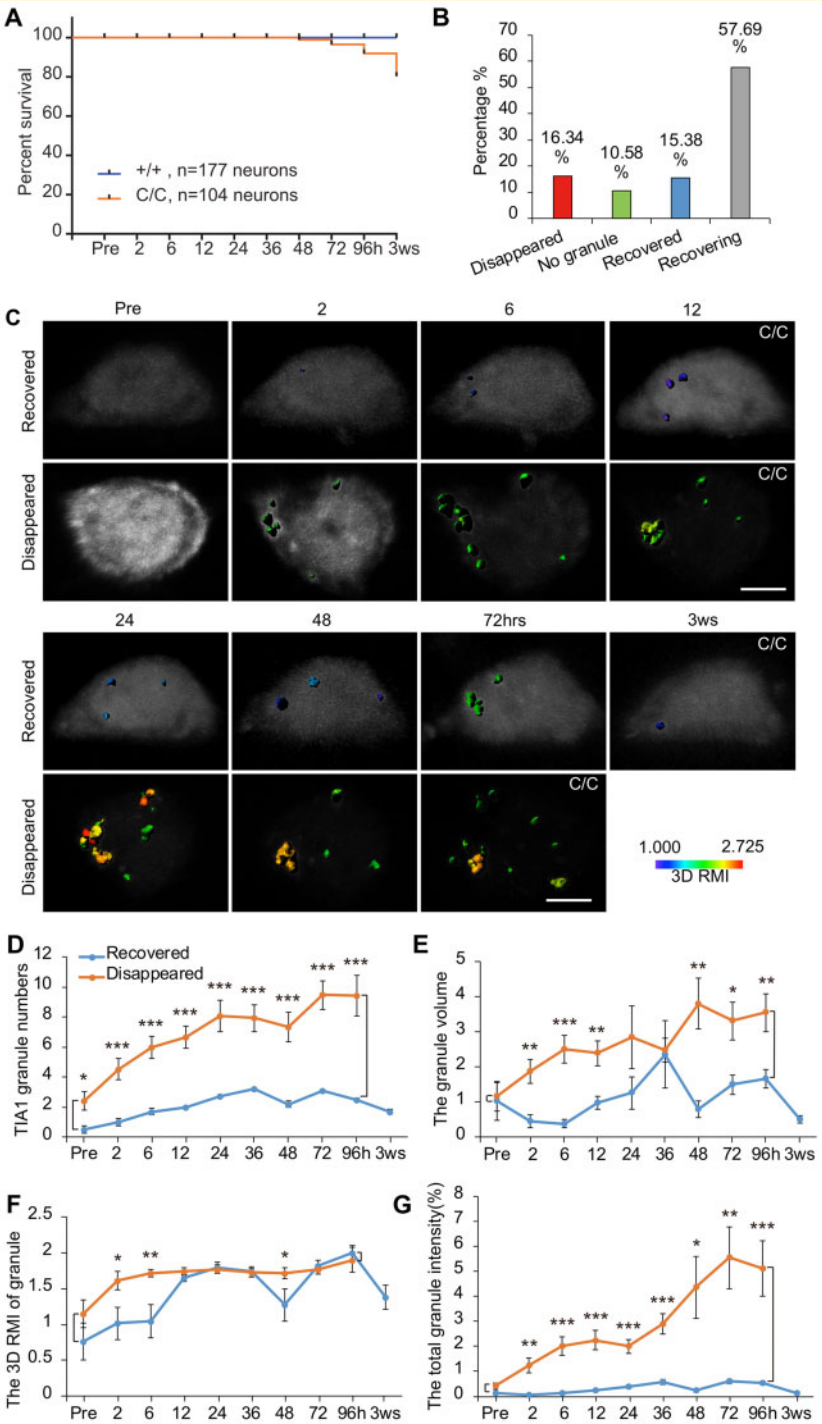

Figure 7 ***In vivo*** **evidence for disappearance of neurons that carry severe abnormalities in TIA1-positive granule processing.** (**A**) The survival rate of TIA1-EGFP positive neurons in the wild-type (+/+) and knock-in mutant (C/C) mice. Seventeen of 104 TIA1-EGFP positive neurons disappeared in the mutant motor cortex. None of the TIA1-EGFP positive neurons (0/177) disappeared in the wild-type motor cortex. (**B**) Four different categories of the TIA1-EGFP positive neurons in the mutant motor cortex according to their responses to the stress treatment. Disappeared = those that disappeared by the end of experiment; no granule formation = those without formation of EGFP-positive granule; recovered = those that the TIA1-EGFP positive granule was recovered 3 weeks after the stress treatment; recovering = those that the TIA1-EGFP-positive granules had not been recovered to pretreatment condition by the end of experiment procedure. (**C**) The 3D reconstruction of TIA1-EGFP positive granules in a recovered and a disappeared mutant (C/C) neuron. The granule 3D RMI was calculated by Imaris. Scale bar = 5 μm. The heat map colour represents the granule 3D RMI. (**D**–**F**) The number (**D**), volume (**E**), and 3D RMI (**F**) of TIA1-EGFP-positive granules were calculated in recovered and disappeared groups after 3D reconstruction. The unit for 3D volume (**E**) is cubic micrometres (μm^3). (**G**) The percentage of total granule intensity (the total TIA1-EGFP granule intensity in the given neuron divided by the overall neuron TIA1-EGFP intensity, %) was calculated in the two groups. The values are presented as mean ± SEM. For the recovered group, 10 TIA1-EGFP positive neurons. For the disappeared group, 14 TIA1-EGFP positive neurons. *$P < 0.05$, **$P < 0.01$, ***$P < 0.001$ (*t*-test, SPSS).

formation, which is stress-dependent and faster than the granule clearance.

Mutant neurons with the granule processing defects disappear days after stress challenge

Interestingly, we observed that the TIA1-EGFP positive neurons disappeared in the FUS mutant cortex as early as 48 h after AS treatment (Fig. 6B and Supplementary Video 1). In contrast, we did not observe any TIA1-EGFP-positive neuron loss in the wild-type animals. By the end of our experimental procedure, 17 of 104 (16.34%) TIA1-EGFP-positive neurons had disappeared (Fig. 7A). We grouped the 104 mutant neurons based on their different cell fates and their performances in the granule processing into at least four categories: (i) those that disappeared; (ii) those with no granule formation at all during the stress challenge (10.58%); (iii) those that recovered, in which the granules returned to wild-type levels 3 weeks after the challenge (15.38%); and (iv) those recovering (57.69%) (Fig. 7B). To determine the difference between the recovered and disappeared mutant neurons in processing of TIA1-positive granules, we reconstructed the 3D shape of TIA1-positive granules in these two categories (Fig. 7C). The granule number differed between the two categories even before the stress challenge (Fig. 7D). The difference became more significant after the stress challenge, indicating that mutant neurons with more TIA1-positive granules were prone to disappear.

To determine the exact size of the granule, we reconstructed granule volumes in the recovered and disappeared groups (Fig. 7C and E). Although a similar volume was observed in the pretreatment condition between the two groups, granule volume was significantly increased ($P < 0.01$, *t*-test) 2 h after the stress treatment in the neurons that disappeared and was maintained at a high level until the neuron disappeared. However, the volume in the recovered group began to increase 24 h after treatment, indicating a delayed expansion of granule size in the group (Fig. 7E). The volume became comparable between the two groups 36 h after treatment; however, that was differentiated at 48 h (Fig. 7E), suggesting increased granule dynamics in the recovered neurons.

Granule dynamics were further documented by the 3D RMI of granules, which had two waves in the recovered group (Fig. 7F). However, like the volume, the 3D RMI rapidly increased within 2 h after the stress treatment in the neurons destined to disappear, and then maintained at a high level until they disappeared (Supplementary Video 2).

To combine the effects of granule number, volume, and TIA1 intensity on cell fate determination, we calculated the percentage of total granule intensity, which was estimated by the ratio of total granule T1A1-EGFP intensity to whole neuron TIA1-EGFP intensity (Fig. 7G). Although the percentage between the two groups was similar before the treatment, it was significantly increased ($P < 0.01$, *t*-test) 2 h after the treatment in the group that would eventually disappear. The percentage was about nine times higher than that of the group that would recover at the time the majority of neurons disappeared (96 h after treatment). Taken together, by using two-photon imaging, we are able to trace the processing of TIA1-positive granules in two groups with different fates following stress, and our data suggest that the increased granule number, volume, and RBP intensity at the early stress response phase determines cell fate.

Discussion

Although hFUS-R521C is one of the most frequent FUS mutations found in ALS (Dormann *et al.*, 2010; Dormann and Haass, 2011), the previously reported hFUS-R521C localization in the non-stress and stress conditions is controversial, probably because of the differences of cell types, stress inducers used, and exogenous FUS expression level (Bosco *et al.*, 2010; Dormann *et al.*, 2010; Li *et al.*, 2013; Japtok *et al.*, 2015; Daigle *et al.*, 2016). In our knock-in mouse spinal cord and primary cultured knock-in motor neuron, we failed to detect mislocalization of FUS to the cytoplasm, but instead saw nucleus-localized mutant FUS, similar to the wild-type FUS in the naïve condition (Supplementary Figs 3 and 7). Similarly, nucleus-localized mutant FUS was detected in the recently reported BAC transgenic ALS mouse models (Lopez-Erauskin *et al.*, 2018). However, we provide compelling evidence that stress challenge differs the subcellular localization of wild-type and ALS mutant FUS in motor neurons *in vitro* and *in vivo*. In culture motor neurons, the stress preferentially induced mutant FUS mislocalization into stress granules (Fig. 4A). *In vivo*, stress induced the upregulation of ubiquitin and co-localization of mislocalized mutant FUS and ubiquitin in the spinal cord motor neurons (Fig. 5C and D), the pathological hallmarks shown in ALS patients (Dormann and Haass, 2011; Renton *et al.*, 2014; Harrison and Shorter, 2017). Finally, we documented the upregulation of eIF3η and G3BP1, stress granule markers, and co-localization between mislocalized mutant FUS and eIF3η as well as between G3BP1 and eIF3η in the spinal cord after stress challenge, supporting stress granule misprocessing *in vivo* (Fig. 5E–G).

Stress not only induces disease-related pathologies, but also worsened motor impairment in our knock-in ALS model (Fig. 5B). On one hand, the stress challenge decreased the travel distance in the wild-type but not FUS mutant animals (Supplementary Fig. 8A). On the other hand, the stress challenge induced a relatively stronger anxiety-like phenotype in the FUS mutant than that in the wild-type animals (Supplementary Fig. 8B), which we believe may drive the mutant animals to travel more. However, the rearing time was significantly reduced in the mutant groups after the stress challenge (Fig. 5B). These results suggested that the stress challenge induces the anxiety-like and hindlimb weakness phenotypes in both the wild-type and FUS mutant animals, but the impairments appear more severe in the mutant

animals. It will be intriguing to learn whether the stress challenge is able to induce the disease pathologies and increase the speed of disease manifestation in the recently reported BAC mutant FUS transgenic and truncated FUS knock-in ALS models (Scekic-Zahirovic *et al.*, 2016, 2017; Devoy *et al.*, 2017; Lopez-Erauskin *et al.*, 2018).

In this study, we noticed that the dosage of mutant *FUS* is not able to phenotypically distinguish the heterozygous and homozygous FUS mutant animals (Figs 2 and 3). By using a TDP-43 ALS disease allele (Q331K) knock-in mouse line, White *et al.* (2018) also showed the similar phenotypic impairments between their heterozygous and homozygous animals. As we claim in this study, ALS mutations and stress are both critical for disease development. However, individual animals are exposed to different levels of environmental and mental stresses and also have different levels of stress response. All of these uncertainties may drive variations in the animals' overall phenotypes and affect our ability to generate enough statistical power to reach conclusions. However, in general, homozygous animals carried slightly more severe phenotypes than heterozygous animals (Figs 2, 3 and Supplementary Fig. 4). In agreement with our *in vivo* data, the homozygous motor neuron cultures also carry slightly more severe stress granule assembly/disassembly defects than that shown in the heterozygous cultures (Fig. 4A–C). However, the motor neuron cultures between C/+ and C/C in aspects of stress granule assembly/disassembly did not show significant difference (Fig. 4A–C), suggesting that the key event to drive the stress granule less dynamics is the mislocalization of mutant FUS into stress granules rather than the dosage of mutant FUS in the stress granules.

One of the open questions in the field is whether neuron loss is caused by the misprocessing of stress granules *in vivo*. Previous studies have attempted to link stress granule misprocessing and mutant FUS toxicity in *in vivo* settings (Mackenzie *et al.*, 2017; Bogaert *et al.*, 2018). To address this question, a tractable approach to trace the whole process of stress granule assembly/disassembly before and after the stress challenge on a valid disease model is needed. Here we establish an *in vivo* setting to trace TIA1-positive granule processing in the same neuron in brain before and after stress challenge (Fig. 6A and B). Without stress challenge, we were not able to distinguish the knock-in mutant and its isogenic wild-type motor neuron *in vivo*, in terms of the TIA1 granule number per neuron and TIA1 intensity per granule (Fig. 6D and E). However, the percentage of cells containing TIA1-positive granules was higher in the mutant group in the pretreatment condition (Fig. 6C), suggesting a slightly higher TIA1-positive granule baseline in the mutant group in naïve condition. However, after stress challenge, the wild-type and mutant neurons behaved differently in the granule processing (Fig. 6C–E). Importantly, the mutant (16.34%), but not wild-type, neurons disappeared days after the challenge and the cell's fate seems to be determined by the TIA1 intensity inside granules, granule numbers, and granule size at the early stress response stage (Fig. 7). Rather than chemical stress, it will be intriguing to test whether the physical or mental stresses that ALS patients are often exposed to are able to drive stress granule misprocessing *in vivo*.

When moving into stress granules, ALS mutant FUS may induce liquid-to-solid phase transition and lead to less dynamic stress granules through its intrinsically disordered region (IDR) (Patel *et al.*, 2015). Alternatively, the mislocalized FUS may increase the multivalent weak interactions through IDR-mediated protein (hetero- or homotypic) and RNA interactions to change the dynamics and properties of liquid–liquid phase separations (LLPS) (Protter and Parker, 2016). Indeed, the intensity of mutant FUS inside stress granules is less dynamic during stress treatment and stress withdrawal (Fig. 4E). In addition, the intensity of mutant FUS inside stress granules is correlated with that of TIA1 and eIF3η in the cultured motor neuron when facing stress (Fig. 4F and Supplementary Fig. 10B). The relocation of mutant FUS into stress granules *in vivo* is evidenced by co-localization between mutant FUS and eIF3η as well as between eIF3η and G3BP1 after stress challenge (Fig. 5E–G). In the mutant motor cortex, TIA1-EGFP intensity inside positive granules is significantly increased shortly after the stress challenge, suggesting the increase of TIA1 level in the granule is the primary effect in the mutant neuron after the stress challenge (Fig. 6E). Compared to the neurons that recovered, the neurons that disappeared in the motor cortex show high TIA1-intensity in granules shortly after stress treatment and maintain lower dynamics (Fig. 7F). The high concentration of RBPs promotes LLPS and the liquid-to-solid phase transition (Molliex *et al.*, 2015; Patel *et al.*, 2015). Therefore, the increase of stress granule formation or/and decease of stress granule disassembly were seen in mutant motor cortex and cultured motor neurons (Figs 4 and 6).

We noticed that upregulation (~3–4-fold) of mutant FUS at early and late disease stages in the mutant spinal cord (Fig. 1E and Supplementary Fig. 2A). A previous study has shown that the protein level of mutant FUS with NLS deletion is upregulated in the spinal cord; particularly, the upregulation appears in the cytoplasmic but not nuclear fraction (Scekic-Zahirovic *et al.*, 2017). The observation fits the FUS autoregulation hypothesis, in which nuclear FUS acts on pre-mRNA splicing/NMD or miRNA production/translation to maintain the FUS protein homeostasis (Zhou *et al.*, 2013; Dini Modigliani *et al.*, 2014). However, ALS mutant FUS is often deficient in nuclear localization and then disrupts these autoregulation mechanisms. Therefore, our R521C mutant FUS may also disrupt the autoregulation mechanisms to increase its protein level through the existing or unidentified molecular pathways.

Stress granule assembly and disassembly are ATP-dependent processes, and several DNA/RNA helicase complexes, which use the energy of ATP hydrolysis to unwind RNA, have been reported to be involved in the transition (Jain *et al.*, 2016). Recently, nuclear-import receptors have been reported to suppress the FUS LLPS and reduction of FUS associated with stress granules (Guo *et al.*, 2018; Hofweber *et al.*, 2018). The persistence of stress granules with high

concentrations of RBP or stress granule components could trigger either the ubiquitin-proteasome or ubiquitin-autophagy pathways for clearance (Monahan *et al.*, 2016; Turakhiya *et al.*, 2018). Indeed, by the end of our *in vivo* experimental procedure, the majority of TIA1-positive granules in the mutant cortex were resolved (Fig. 6D). It will be interesting to examine whether those molecules or molecular pathways contribute to the stress granule assembly/disassembly/clearance in motor neurons *in vivo*, by using our *in vivo* setting and knock-in animal.

Acknowledgements

We thank staff members in the Laboratory Animal Research Center (Tsinghua University) and the Animal Facility in Shanghai (National Facility for Protein Science in Shanghai, Zhangjiang Lab, China) for mouse housing. We thank the Imaging Core Facility, the Technology Center for Protein Sciences (Tsinghua University) for assistance on confocal imaging (Nikon A1) and Imaris software data analysis. Drs Charles Jennings, Songhai Shi, Yongbin Yan, Yi Zhong, Juntao Gao, Michael Q. Zhang, and Robert Burgess for comments and discussions on the manuscript. Dr Yanbo Chen, Cheng Cheng, and Shijiao Zhang for help on the experiments.

Funding

This work is supported by the National Natural Science Foundation of China (NSFC grants, 31571097 and 81371361), the Junior 1000 Talents Program (Government of China), the School of Medicine at Tsinghua, the School of Life Sciences at Tsinghua, Tsinghua-Peking Joint Center for Life Sciences, IDG/McGovern Institute for Brain Research at Tsinghua (Brain +X project), and the Amyotrophic Lateral Sclerosis Association (ALSA grant, 16-IIP-284).

Competing interests

The authors report no competing interests.

Supplementary material

Supplementary material is available at *Brain* online.

References

Aulas A, Vande Velde C. Alterations in stress granule dynamics driven by TDP-43 and FUS: a link to pathological inclusions in ALS? Front Cell Neurosci 2015; 9: 423.

Becker LA, Huang B, Bieri G, Ma R, Knowles DA, Jafar-Nejad P, et al. Therapeutic reduction of ataxin-2 extends lifespan and reduces pathology in TDP-43 mice. Nature 2017; 544: 367–71.

Bogaert E, Boeynaems S, Kato M, Guo L, Caulfield TR, Steyaert J, et al. Molecular dissection of FUS points at synergistic effect of low-complexity domains in toxicity. Cell Rep 2018; 24: 529–37 e4.

Bosco DA, Lemay N, Ko HK, Zhou H, Burke C, Kwiatkowski TJ Jr, et al. Mutant FUS proteins that cause amyotrophic lateral sclerosis incorporate into stress granules. Hum Mol Genet 2010; 19: 4160–75.

Buchan JR, Kolaitis RM, Taylor JP, Parker R. Eukaryotic stress granules are cleared by autophagy and Cdc48/VCP function. Cell 2013; 153: 1461–74.

Chew J, Gendron TF, Prudencio M, Sasaguri H, Zhang YJ, Castanedes-Casey M, et al. Neurodegeneration. C9ORF72 repeat expansions in mice cause TDP-43 pathology, neuronal loss, and behavioral deficits. Science 2015; 348: 1151–4.

Colombrita C, Zennaro E, Fallini C, Weber M, Sommacal A, Buratti E, et al. TDP-43 is recruited to stress granules in conditions of oxidative insult. J Neurochem 2009; 111: 1051–61.

Daigle JG, Krishnamurthy K, Ramesh N, Casci I, Monaghan J, McAvoy K, et al. Pur-alpha regulates cytoplasmic stress granule dynamics and ameliorates FUS toxicity. Acta Neuropathol 2016; 131: 605–20.

Devoy A, Kalmar B, Stewart M, Park H, Burke B, Noy SJ, et al. Humanized mutant FUS drives progressive motor neuron degeneration without aggregation in 'FUSDelta14' knockin mice. Brain 2017; 140: 2797–805.

Dini Modigliani S, Morlando M, Errichelli L, Sabatelli M, Bozzoni I. An ALS-associated mutation in the FUS 3'-UTR disrupts a microRNA-FUS regulatory circuitry. Nat Commun 2014; 5: 4335.

Dormann D, Haass C. TDP-43 and FUS: a nuclear affair. Trends Neurosci 2011; 34: 339–48.

Dormann D, Rodde R, Edbauer D, Bentmann E, Fischer I, Hruscha A, et al. ALS-associated fused in sarcoma (FUS) mutations disrupt transportin-mediated nuclear import. EMBO J 2010; 29: 2841–57.

Drepper C, Herrmann T, Wessig C, Beck M, Sendtner M. C-terminal FUS/TLS mutations in familial and sporadic ALS in Germany. Neurobiol Aging 2011; 32: 548 e1–4.

Ebstein SY, Yagudayeva I, Shneider NA. Mutant TDP-43 causes early-stage dose-dependent motor neuron degeneration in a TARDBP knockin mouse model of ALS. Cell Rep 2019; 26: 364–73.e4.

Elden AC, Kim HJ, Hart MP, Chen-Plotkin AS, Johnson BS, Fang X, et al. Ataxin-2 intermediate-length polyglutamine expansions are associated with increased risk for ALS. Nature 2010; 466: 1069–75.

Flora SJ. Arsenic-induced oxidative stress and its reversibility following combined administration of N-acetylcysteine and meso 2,3-dimercaptosuccinic acid in rats. Clin Exp Pharmacol Physiol 1999; 26: 865–9.

Fratta P, Sivakumar P, Humphrey J, Lo K, Ricketts T, Oliveira H, et al. Mice with endogenous TDP-43 mutations exhibit gain of splicing function and characteristics of amyotrophic lateral sclerosis. EMBO J 2018; 37:

Guo L, Kim HJ, Wang H, Monaghan J, Freyermuth F, Sung JC, et al. Nuclear-import receptors reverse aberrant phase transitions of RNA-binding proteins with prion-like domains. Cell 2018; 173: 677–92.e20.

Gurney ME, Pu H, Chiu AY, Dal Canto MC, Polchow CY, Alexander DD, et al. Motor neuron degeneration in mice that express a human Cu, Zn superoxide dismutase mutation. Science 1994; 264: 1772–5.

Harrison AF, Shorter J. RNA-binding proteins with prion-like domains in health and disease. Biochem J 2017; 474: 1417–38.

Hofweber M, Hutten S, Bourgeois B, Spreitzer E, Niedner-Boblenz A, Schifferer M, et al. Phase separation of FUS is suppressed by its nuclear import receptor and arginine methylation. Cell 2018; 173: 706–19.e13.

Huang C, Zhou H, Tong J, Chen H, Liu YJ, Wang D, et al. FUS transgenic rats develop the phenotypes of amyotrophic lateral sclerosis and frontotemporal lobar degeneration. PLoS Genet 2011; 7: e1002011.

Ito Y, Ofengeim D, Najafov A, Das S, Saberi S, Li Y, et al. RIPK1 mediates axonal degeneration by promoting inflammation and necroptosis in ALS. Science 2016; 353: 603–8.

Jain S, Wheeler JR, Walters RW, Agrawal A, Barsic A, Parker R. ATPase-modulated stress granules contain a diverse proteome and substructure. Cell 2016; 164: 487–98.

Japtok J, Lojewski X, Naumann M, Klingenstein M, Reinhardt P, Sterneckert J, et al. Stepwise acquirement of hallmark neuropathology in FUS-ALS iPSC models depends on mutation type and neuronal aging. Neurobiol Dis 2015; 82: 420–9.

Jia Y, Jucius TJ, Cook SA, Ackerman SL. Loss of Clcc1 results in ER stress, misfolded protein accumulation, and neurodegeneration. J Neurosci 2015; 35: 3001–9.

Jonsson PA, Graffmo KS, Andersen PM, Brannstrom T, Lindberg M, Oliveberg M, et al. Disulphide-reduced superoxide dismutase-1 in CNS of transgenic amyotrophic lateral sclerosis models. Brain 2006; 129: 451–64.

Juarez-Reyes A, Jimenez-Capdeville ME, Delgado JM, Ortiz-Perez D. Time course of arsenic species in the brain and liver of mice after oral administration of arsenate. Arch Toxicol 2009; 83: 557–63.

Kedersha N, Stoecklin G, Ayodele M, Yacono P, Lykke-Andersen J, Fritzler MJ, et al. Stress granules and processing bodies are dynamically linked sites of mRNP remodeling. J Cell Biol 2005; 169: 871–84.

Kedersha NL, Gupta M, Li W, Miller I, Anderson P. RNA-binding proteins TIA-1 and TIAR link the phosphorylation of eIF-2 alpha to the assembly of mammalian stress granules. J Cell Biol 1999; 147: 1431–42.

Kim HJ, Kim NC, Wang YD, Scarborough EA, Moore J, Diaz Z, et al. Mutations in prion-like domains in hnRNPA2B1 and hnRNPA1 cause multisystem proteinopathy and ALS. Nature 2013; 495: 467–73.

Kwiatkowski TJ Jr, Bosco DA, Leclerc AL, Tamrazian E, Vanderburg CR, Russ C, et al. Mutations in the FUS/TLS gene on chromosome 16 cause familial amyotrophic lateral sclerosis. Science 2009; 323: 1205–8.

Lagier-Tourenne C, Polymenidou M, Cleveland DW. TDP-43 and FUS/TLS: emerging roles in RNA processing and neurodegeneration. Hum Mol Genet 2010; 19: R46–64.

Li J, Duan X, Dong D, Zhang Y, Zhao L, Li W, et al. Tissue-specific distributions of inorganic arsenic and its methylated metabolites, especially in cerebral cortex, cerebellum and hippocampus of mice after a single oral administration of arsenite. J Trace Elem Med Biol 2017; 43: 15–22.

Li YR, King OD, Shorter J, Gitler AD. Stress granules as crucibles of ALS pathogenesis. J Cell Biol 2013; 201: 361–72.

Ling SC, Polymenidou M, Cleveland DW. Converging mechanisms in ALS and FTD: disrupted RNA and protein homeostasis. Neuron 2013; 79: 416–38.

Liu SX, Athar M, Lippai I, Waldren C, Hei TK. Induction of oxyradicals by arsenic: implication for mechanism of genotoxicity. Proc Natl Acad Sci USA 2001; 98: 1643–8.

Liu-Yesucevitz L, Bilgutay A, Zhang YJ, Vanderweyde T, Citro A, Mehta T, et al. Tar DNA binding protein-43 (TDP-43) associates with stress granules: analysis of cultured cells and pathological brain tissue. PLoS One 2010; 5: e13250.

Lopez-Erauskin J, Tadokoro T, Baughn MW, Myers B, McAlonis-Downes M, Chillon-Marinas C, et al. ALS/FTD-linked mutation in FUS suppresses intra-axonal protein synthesis and drives disease without nuclear loss-of-function of FUS. Neuron 2018; 100: 816–30.e7.

Mackenzie IR, Nicholson AM, Sarkar M, Messing J, Purice MD, Pottier C, et al. TIA1 mutations in amyotrophic lateral sclerosis and frontotemporal dementia promote phase separation and alter stress granule dynamics. Neuron 2017; 95: 808–16.e9.

Maharana S, Wang J, Papadopoulos DK, Richter D, Pozniakovsky A, Poser I, et al. RNA buffers the phase separation behavior of prion-like RNA binding proteins. Science 2018; 360: 918–21.

Mitchell JC, McGoldrick P, Vance C, Hortobagyi T, Sreedharan J, Rogelj B, et al. Overexpression of human wild-type FUS causes progressive motor neuron degeneration in an age- and dose-dependent fashion. Acta Neuropathol 2013; 125: 273–88.

Molliex A, Temirov J, Lee J, Coughlin M, Kanagaraj AP, Kim HJ, et al. Phase separation by low complexity domains promotes stress granule assembly and drives pathological fibrillization. Cell 2015; 163: 123–33.

Monahan Z, Shewmaker F, Pandey UB. Stress granules at the intersection of autophagy and ALS. Brain Res 2016; 1649: 189–200.

Patel A, Lee HO, Jawerth L, Maharana S, Jahnel M, Hein MY, et al. A liquid-to-solid phase transition of the ALS protein FUS accelerated by disease mutation. Cell 2015; 162: 1066–77.

Platt RJ, Chen S, Zhou Y, Yim MJ, Swiech L, Kempton HR, et al. CRISPR-Cas9 knockin mice for genome editing and cancer modeling. Cell 2014; 159: 440–55.

Protter DS, Parker R, Principles and properties of stress granules. Trends Cell Biol 2016; 26: 668–79.

Qiu H, Lee S, Shang Y, Wang WY, Au KF, Kamiya S, et al. ALS-associated mutation FUS-R521C causes DNA damage and RNA splicing defects. J Clin Invest 2014; 124: 981–99.

Renton AE, Chio A, Traynor BJ. State of play in amyotrophic lateral sclerosis genetics. Nat Neurosci 2014; 17: 17–23.

Scekic-Zahirovic J, Oussini HE, Mersmann S, Drenner K, Wagner M, Sun Y, et al. Motor neuron intrinsic and extrinsic mechanisms contribute to the pathogenesis of FUS-associated amyotrophic lateral sclerosis. Acta Neuropathol 2017; 133: 887–906.

Scekic-Zahirovic J, Sendscheid O, El Oussini H, Jambeau M, Sun Y, Mersmann S, et al. Toxic gain of function from mutant FUS protein is crucial to trigger cell autonomous motor neuron loss. EMBO J 2016; 35: 1077–97.

Shalem O, Sanjana NE, Zhang F. High-throughput functional genomics using CRISPR-Cas9. Nat Rev Genet 2015; 16: 299–311.

Shi H, Shi X, Liu KJ. Oxidative mechanism of arsenic toxicity and carcinogenesis. Mol Cell Biochem 2004; 255: 67–78.

Sproviero W, La Bella V, Mazzei R, Valentino P, Rodolico C, Simone IL, et al. FUS mutations in sporadic amyotrophic lateral sclerosis: clinical and genetic analysis. Neurobiol Aging 2012; 33: 837.e1–5.

Suzuki N, Aoki M, Warita H, Kato M, Mizuno H, Shimakura N, et al. FALS with FUS mutation in Japan, with early onset, rapid progress and basophilic inclusion. J Hum Genet 2010; 55: 252–4.

Swarup V, Julien JP. ALS pathogenesis: recent insights from genetics and mouse models. Prog Neuropsychopharmacol Biol Psychiatry 2011; 35: 363–9.

Swarup V, Phaneuf D, Bareil C, Robertson J, Rouleau GA, Kriz J, et al. Pathological hallmarks of amyotrophic lateral sclerosis/frontotemporal lobar degeneration in transgenic mice produced with TDP-43 genomic fragments. Brain 2011; 134: 2610–26.

Turakhiya A, Meyer SR, Marincola G, Bohm S, Vanselow JT, Schlosser A, et al. ZFAND1 recruits p97 and the 26S proteasome to promote the clearance of arsenite-induced stress granules. Mol Cell 2018; 70: 906–19.e7.

Vance C, Rogelj B, Hortobagyi T, De Vos KJ, Nishimura AL, Sreedharan J, et al. Mutations in FUS, an RNA processing protein, cause familial amyotrophic lateral sclerosis type 6. Science 2009; 323: 1208–11.

Wegorzewska I, Bell S, Cairns NJ, Miller TM, Baloh RH. TDP-43 mutant transgenic mice develop features of ALS and frontotemporal lobar degeneration. Proc Natl Acad Sci USA 2009; 106: 18809–14.

Wheeler JR, Matheny T, Jain S, Abrisch R, Parker R. Distinct stages in stress granule assembly and disassembly. Elife 2016; 5.

White MA, Kim E, Duffy A, Adalbert R, Phillips BU, Peters OM, et al. TDP-43 gains function due to perturbed autoregulation in a Tardbp knock-in mouse model of ALS-FTD. Nat Neurosci 2018; 21: 552–63.

Xie H, Liu Y, Zhu Y, Ding X, Yang Y, Guan JS. In vivo imaging of immediate early gene expression reveals layer-specific memory traces in the mammalian brain. Proc Natl Acad Sci USA 2014; 111: 2788–93.

Yamamoto-Watanabe Y, Watanabe M, Okamoto K, Fujita Y, Jackson M, Ikeda M, et al. A Japanese ALS6 family with mutation R521C in the FUS/TLS gene: a clinical, pathological and genetic report. J Neurol Sci 2010; 296: 59–63.

Zhang YJ, Gendron TF, Ebbert MTW, O'Raw AD, Yue M, Jansen-West K, et al. Poly(GR) impairs protein translation and stress granule dynamics in C9orf72-associated frontotemporal dementia and amyotrophic lateral sclerosis. Nat Med 2018; 24: 1136–42.

Zhou Y, Liu S, Liu G, Ozturk A, Hicks GG. ALS-associated FUS mutations result in compromised FUS alternative splicing and autoregulation. PLoS Genet 2013; 9: e1003895.